Front. Chem. Sci. Eng. 2023, 17(7): 853−866
https://doi.org/10.1007/s11705-022-2256-x

RESEARCH ARTICLE

Dialdehyde cellulose nanocrystal cross-linked chitosan foam with high adsorption capacity for removal of acid red 134

Xiuzhi Tian[1], Rui Yang[1], Chuanyin Xiong[1], Haibo Deng[2], Yonghao Ni[3], Xue Jiang (✉)[1]

1 College of Bioresource Chemical and Materials Engineering, Shaanxi University of Science and Technology, Xi'an 710021, China
2 College of Textile Science and Engineering, Jiangnan University, Wuxi 214122, China
3 Department of Chemical Engineering and Limerick Pulp and Paper Centre, University of New Brunswick, Fredericton, NB E3B 5A3, Canada

Abstract The discharge of large amounts of dye-containing wastewater seriously threats the environment. Adsorbents have been adopted to remove these dyes present in the wastewater. However, the high adsorption capacity, predominant pH-responsibility, and excellent recyclability are three challenges to the development of efficient adsorbents. The poly(acryloxyethyl trimethylammonium chloride)-graft-dialdehyde cellulose nanocrystals were synthesized in our work. Subsequently, the cationic dialdehyde cellulose nanocrystal cross-linked chitosan nanocomposite foam was fabricated via freeze-drying of the hydrogel. Under the optimal ratio of the cationic dialdehyde cellulose nanocrystal/chitosan (w/w) of 12/100, the resultant foam (Foam-12) possesses excellent absorption properties, such as high porosity, high content of active sites, strong acid resistance, and high amorphous region. Then, Foam-12 was applied as an eco-friendly adsorbent to remove acid red 134 (a representative of anionic dyes) from aqueous solutions. The maximum dye adsorption capacity of 1238.1 $mg \cdot g^{-1}$ is achieved under the conditions of 20 $mg \cdot L^{-1}$ adsorbents, 100 $mg \cdot L^{-1}$ dye, pH 3.5, 24 h, and 25 °C. The dominant adsorption mechanism for the anionic dye adsorption is electrostatic attraction, and Foam-12 can effectively adsorb acid red 134 at pH 2.5–5.5 and be desorbed at pH 8. Its easy recovery and good reusability are verified by the repeated acid adsorption–alkaline desorption experiments.

Keywords chitosan foam, cellulose nanocrystals, acid red 134, adsorption

1 Introduction

Synthetic dyes have been widely applied in various industries, such as textile, paper, leather, food, printing, and plastics factories [1]. A wide range of dyes are used in these industries for coloring or manufacturing, producing a vast amount of dye wastewater every day. The dye-containing wastewater poses not only health hazards to humans but also an environmental impact on the ecology if discharged without treatment [2]. Regrettably, the color of dye wastewater even after going through a multi-step treatment process is still deep, which suggests that substantial amount of residual dyes still exist [3]. Thus, a further decolorization of the multi-step treated water is required. Most dyes in wastewater are difficult to be degraded by common chemical or biological reagents because they are chemically stable and non-biodegradable. Even if degraded, there is a great possibility of producing more toxic products from these dyes [4,5]. Many dyes are negatively charged (so-called anionic dyes), such as acid dyes and direct dyes. To remove these anionic dyes, positively charged adsorbents should be effective, thanks to their electrostatic attraction [6]. Although several adsorbents have been reported in the literature, their separation from aqueous metrics could still be challenging due to their micro or nano sizes, which limits their application potential. It is highly desirable to develop biopolymer-based adsorbent with high adsorption/desorption efficiency, pH independence, and convenient separation ability for discoloring these wastewaters [7].

Chitosan is a low-cost biopolymer with unique characteristics of biocompatibility, biodegradability, non-toxicity, and non-immunogenicity [8,9]. Chitosan offers outstanding adsorption and desorption of negatively-

Received July 8, 2022; accepted September 7, 2022

E-mail: jiangx@sust.edu.cn

charged dyes due to its amino groups [10,11]. However, chitosan cannot function as a solid adsorbent for decolorization of the dye-containing wastewater under acid conditions because it dissolves in acid solutions. Although the chitosan-based gel beads, microsphere, powders, or particles prepared by the cross-linking technique can solve this problem [10], it is troublesome to separate these adsorbents from the purified water at the end of the dye adsorption process unless they are magnetically functionalized [12,13]. On the other hand, the cross-linked chitosan adsorbent in the form of foam, sponge matrices, porous membrane, or aerogel can be better choices for the adsorption of negatively-charged dyes, as they do not require post-treatment like filtration [14–16]. In addition, the presence of these rich micro- and mesopores in the cross-linked chitosan can facilitate the mass transfer in the process of dye adsorption. Nevertheless, they still have some shortcomings. Firstly, these adsorbents are not eco-friendly because the poorly biocompatible and highly cytotoxic agents, e.g., glutaraldehyde, tripolyphosphate, H_2SO_4, epichlorohydrin, and dimethyloldihydroxyethyleneurea tetraethoxysilane are often adopted for the cross-linking reaction [17]. Secondly, the amount of glucosamine that could be accessed by the dyes is reduced because a part of them participates in the cross-linking reaction. In view of the above, other bio-origin reagents with good biocompatibility and low cytotoxicity should be selected as the cross-linker for chitosan to prepare an eco-friendly adsorbent. Meanwhile, cationic groups for immobilization of the negatively-charged dyes should be introduced into the cross-linker to make up the loss of glucosamine of chitosan in the cross-linking reaction. Finally, developing biomass-based reagents that contain both cross-linking groups and cationic groups to compound with chitosan is expected to solve the shortcomings of the existing cross-linked chitosan adsorbents.

Cellulose nanocrystals (CNCs) that was surface-quaternized have been proved to offer high adsorption efficiency toward anionic dyes [18,19], but there are no reactive groups on their surface for cross-linking reaction. Dialdehyde CNCs (DACNCs) prepared by the method of $NaIO_4$ oxidation are green cross-linker for chitosan, but no cationic groups on their surface [20]. Hereby, CNCs with both dialdehyde and quaternary ammonium groups are hopeful to prepare the chitosan-based adsorbent with the aimed properties, such as high adsorption efficiency, and easy desorption and separation after adsorption. Currently, there is no relevant research in this particular issue. In our previous study, the surface-quaternized CNCs were prepared through the Schiff-base reaction between the aldehyde groups (–CHO) on DACNCs and the amino groups ($–NH_2$) in Girard's reagent T [$H_2NNHC(=O)CH_2N^+(CH_3)_3Cl^-$] [19]. There are no flocs that appeared during the mixing of the quaternary ammonium functionalized CNC suspension with the chitosan acetic acid solution. Accordingly, a dense nanocomposite film forms after solvent evaporation. Only very limited aldehyde groups are present on the surface of the cationic CNCs prepared by this method, which negatively affects the cross-linking capacity for chitosan.

In the present study, a novel route to synthesize CNCs containing both considerable dialdehyde groups and cationic polyelectrolyte branches was proposed in Scheme 1. Specifically, CNCs from the H_2SO_4 hydrolysis of degreasing cotton are oxidized by $NaIO_4$ to yield DACNCs. Then acryloyloxyethyltrimethyl ammonium chloride (AETMAC) is grafted on the hydroxyl groups on DACNCs by radical polymerization. Radical polymerization is adopted in order to protect the dialdehyde groups on DACNCs [21]. The obtained Poly(AETMAC)-graft-DACNCs (PAETMAC-*g*-DACNCs) serve as nanofillers and cross-linking agents for chitosan. In this case, the PAETAMC-*g*-DACNC suspension is mixed with the chitosan acetic acid solution till the hydrogel forms, which is also presented in Scheme 1. The Schiff-base reaction between the dialdehyde groups on PAETMAC-*g*-DACNCs and the glucosamine groups of chitosan leads to the formation of a highly hydrated cross-linking network. Ultimately, the hydrogel is freeze-dried to yield the nanocomposite foam. The cationic PAETMAC side chains of CNC are assumed to make up for the loss of glucosamine in the cross-linking reaction between chitosan and PAETMAC-*g*-DACNCs, and porous chitosan foam formed. Besides, the porous foams possess millions of tiny pores both in their bulk and on their surface. These pores are beneficial for mass penetration during the dye adsorption process.

The potential and highly-improved acid resistance, high adsorption efficiency, easy recovery and good reusability of these polysaccharide-based adsorbents, are fully predictable. The chemical composition and crystalline structure of PAETMAC-*g*-DACNCs were characterized by Fourier transform infrared spectroscopy (FTIR) and X-ray diffraction (XRD) patterns, the morphology was observed through a transmission electron microscope (TEM), and the size and Zeta potential (ζ) were measured using a Zeta-Plus Analyzer. Nanocomposite foams were fabricated by adjusting the PAETMAC-*g*-DACNCs/chitosan weight ratio in the mixture (3/100, 6/100, 9/100, and 12/100). The cross-linking degrees between PAETMAC-*g*-DACNCs and chitosan were calculated in terms of the glucosamine percentage tests. The pores were observed from scanning electron microscopy (SEM) images of the cross-section. Meanwhile, the porosities were measured gravimetrically using the ethanol adsorption method. The acid resistance was discussed based on the saturated swelling ratios immersed in water at 25 °C and varied pH values. The PAETAMC-*g*-DACNCs/chitosan nanocomposite foam at PAETAMC-*g*-DACNCs/chitosan weight ratio of 12/100 was used as an absorbent for removing acid red (AR) 134 from aqueous

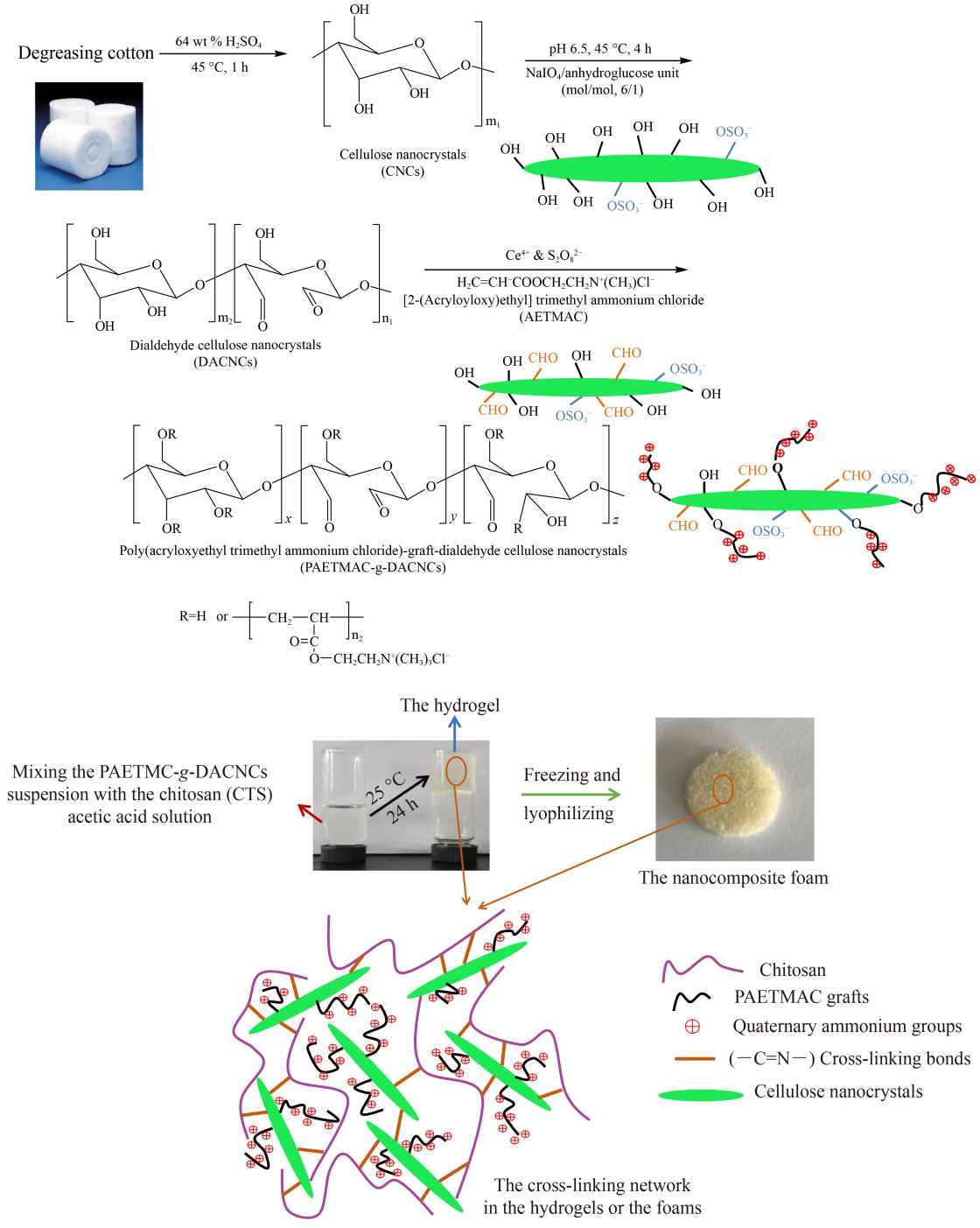

Scheme 1 The route to synthesize CNCs containing dialdehyde and quaternary ammonium groups and prepare their filled and cross-linked chitosan foam.

solution, the adsorption and desorption performances were investigated in detail.

2 Experimental

2.1 Reagents and materials

Degreasing cotton was purchased from Hualu sanitary materials Co., Ltd. Chitosan powder (average M_n 1000 kDa, DD 70%–85%) was purchased from Zhejiang Golden Shell Pharmaceutical Co., Ltd. Ammonium cerium (IV) nitrate, potassium persulfate, H_2SO_4, hydrochloric acid (HCl), acetic acid and NaOH, analytical grade, were purchased from Sinopharm Chemical Reagent Co., Ltd. $NaIO_4$, hydroxylamine hydrochloride, AETMAC (80% solution in water) and cellulose dialysis membrane were purchased from Sigma-Aldrich. AR 134

($C_{40}H_{34}N_4Na_2O_{12}S_2$), a gift from a dye manufacturing unit in China, was used without further purification.

2.2 Preparation of the CNC, DACNC, and PAETMAC-*g*-DACNC suspension

Degreasing cotton was adopted as the raw material. The specific preparation process using the method of H_2SO_4 hydrolysis was referred to our previous work [22]. Part of the collected suspension was freeze-dried for characterization.

The prescribed amount of $NaIO_4$ (6 mol per mol of anhydroglucose unit) was mixed with the CNC suspension. The mixture was carefully wrapped in an aluminum foil and vigorously stirred at 45 °C in the dark for 4 h. Ethylene glycol was added into the mixture to quench the oxidation reaction. The mixture was dialyzed against deionized water for 4 d to remove any unreacted reagents and by-products. Part of the collected suspension was freeze-dried for characterization.

The free radical polymerization of AETMAC at the surface hydroxyl groups on DACNCs was initiated by ammonium ceric nitrate and potassium persulfate. In summary, the DACNC suspension (100 mL, 20 g·L^{-1}), 0.001 mol·L^{-1} of ammonium ceric nitrate and 0.002 mol·L^{-1} of potassium persulfate were transferred into a three-necked bottle, which was placed in a water bath maintained at 50 °C. Then the suspension was purged with nitrogen gas for 10 min under continuous stirring. After that, the required amount of AETMAC (twice the weight of DACNCs) was added and the reaction was conducted for 3 h with N_2 flowing. At the end of reactions, the suspension was dialyzed against deionized water for 3 d to remove any unreacted reagents and by-products. The suspension was centrifugated at 5000 r·min^{-1} for 10 min. The precipitate was purified by Soxhlet extraction with ethanol for 2 d to remove the unreacted monomer and homo-polymer of PAETMAC. Part of the collected product of PAETMAC-*g*-DACNCs was freeze-dried for characterization.

2.3 Fabrication of the PAETMAC-*g*-DACNC filled and cross-linked chitosan nanocomposite foams

Chitosan powder (20 g) was dissolved in 1000 mL of 1.5% (w/v) acetic acid solution. It was ultrasonically mixed with 80 mL of the PAETMAC-*g*-DACNC suspension with certain solid content (0–3.6 g·L^{-1}) for 10 min. After vacuum degassing, the mixture was poured into a Petri dish and kept at 25 °C for one day to allow the fully cross-linking reaction between PAETMAC-*g*-DACNCs and chitosan. The formed hydrogel was frozen at –80 °C for 2 h and lyophilized at –60 °C under vacuum (less than 10 Pa). The freeze-dried sample was washed with 0.1 mol·L^{-1} NaOH followed by deionized water rinsing until reaching the solution's neutral pH. Finally, the sample was freeze-dried once again and the PAETMAC-*g*-DACNC filled and cross-linked chitosan nanocomposite foam was acquired.

The weight ratio of PAETMAC-*g*-DACNCs relative to chitosan in the nanocomposite foam was varied at 0/100 (chitosan only), 3/100, 6/100, 9/100, and 12/100, and the prepared PAETMAC-*g*-DACNCs/chitosan nanocomposite foams were abbreviated as Foam-0, Foam-3, Foam-6, Foam-9, and Foam-12, respectively.

2.4 Methods of characterization

2.4.1 Instrumental analysis

FTIR spectra were recorded on a Nicolet iS10 spectrometer in the optical range of 500–4000 cm^{-1} by averaging 32 scans at a resolution of 4 cm^{-1}. The XRD patterns in the 2θ range of 4° to 45° were acquired on a D8 X-ray diffractometer (Bruker, Germany) with Cu-Kα radiation (wavelength: 0.154 nm) at 40 mA, 40 kV and 2°·min^{-1}. The degree of the crystallinity was characterized in terms of the crystallinity index (*CrI*, %) as Eq. (1):

$$CrI = \frac{I_{200} - I_{\mathrm{am}}}{I_{200}} \times 100\%, \tag{1}$$

where I_{200} and I_{am} are the diffraction intensity of crystalline plane of (200) at 22.6° and that of amorphous fraction of cellulose at 18.0°.

The cross-section of each sample was fractured in liquid nitrogen and sputtered with a thin layer of gold. It was observed by SEM (SU-1510, Hitachi, Japan) with an accelerating voltage of 5 kV. The TEM images of CNCs, DACNCs and PAETMAC-*g*-DACNCs were obtained by TEM (JEM-2100, Japan) operating at 80 kV.

2.4.2 The testing of physical chemical parameters of PAETMAC-*g*-DACNCs

The amount of free aldehyde groups, particle size, cationicity (*a*) and ζ-values were determined by the method reported in the literature [22,23].

The density (ρ_2, g·mL^{-1}) and porosity (%) of each sample were measured gravimetrically using ethanol adsorption [24], which were calculated by Eq. (2) and Eq. (3), respectively:

$$\rho_1 = \rho_2 \frac{W_1}{W_1 - W_3 - W_4}, \tag{2}$$

$$\text{Porosity}\,(\%) = \frac{(W_2 - W_1)\rho_1}{W_1\rho_2 + (W_2 - W_1)\rho_1} \times 100\%, \tag{3}$$

where W_1, W_2, W_3 and W_4 are the weights of the dried sample, sample with adsorbed ethanol, pycnometer with the sample and ethanol, and pycnometer with ethanol (g), respectively; ρ_1 and ρ_2 are the densities of sample and ethanol (g·mL^{-1}), respectively.

The weight percentage of glucosamine in each sample

was measured by using pH-titration, which reflects the cross-linking degree of PAETMAC-*g*-DACNCs with chitosan [12]. The weight percentage of glucosamine (W_{NH_2}, %) was calculated by Eq. (4):

$$W_{NH_2}(\%) = \frac{M_{NaOH} \times (V_2 - V_1) \times 161}{W} \times 100\%, \quad (4)$$

where M_{NaOH} is the molarity of NaOH solution, V_1 and V_2 are the volumes to neutralize the excess of HCl and the protonated glucosamine groups, respectively, 161 is the molecular weight of glucosamine of chitosan and W is the mass of dried sample before titration. The cross-linking degree between chitosan and PAETMAC-*g*-DACNCs (D_c, %) in each sample was determined as Eq. (5):

$$D_C(\%) = \frac{W'_{NH_2} - W_{NH_2}}{W'_{NH_2}} \times 100\%, \quad (5)$$

where W_{NH_2} and W'_{NH_2} are the weight percentages of glucosamine in the PAETMAC-*g*-DACNCs/chitosan nanocomposite foam and the pure chitosan foam without PAETMAC-*g*-DACNCs, respectively.

At 25 °C, the dried sample with known weight (W_0, g) was immersed in deionized water (at pH 3.5, 5 or 6.5) for 3 d, the swollen sample was taken out, slightly pressed between two blotting papers to remove surface water, and immediately weighed (W_s, g). Each sample was analyzed three times. The swelling ratio (%) was calculated based on Eq. (6):

$$\text{Swelling ratio}(\%) = \frac{W_S - W_0}{W_0} \times 100\%. \quad (6)$$

2.4.3 Dye adsorption and desorption

The effect of pH on adsorption was measured by using the Foam-12 adsorbent and AR 134 dye. The details of adsorption experiments were referred to our previous work [25]. The concentrations of AR 134 in the initial and treated solution were measured by UV–Vis spectrophotometric absorbance at 540 nm wavelength. The percentage of dye removal (DR, %) was calculated by Eq. (7), and the amount of adsorbed dye per unit mass, Q (mg·g^{-1}), was calculated by Eq. (8):

$$DR(\%) = \left(1 - \frac{V_r c_r}{V_0 c_0}\right) \times 100\%, \quad (7)$$

$$Q = \frac{V_0 c_0 - V_r c_r}{W}, \quad (8)$$

where V_0 and V_r are the volumes (L) of the initial dye solution and the dye solution after adsorption, respectively, c_0 and c_r are the concentrations (mg·L^{-1}) of the initial dye solution and the dye solution after adsorption, respectively, and W is the weight (g) of the adsorbent.

To reveal adsorption kinetics and isotherm of AR 134 onto Foam-12, experiments were conducted with 20 mg of adsorbent and 100 mL of dye solution at pH 3.5 and 25 °C. Other experimental details were also referred to our previous work [25]. The amount of dye adsorbed on the adsorbent at time t, Q_t (mg·g^{-1}) and the equilibrium adsorption capacity, Q_e (mg·g^{-1}), were calculated by Eqs. (9) and (10), respectively:

$$Q_t = \frac{V_0 c_0 - V_t c_t}{W}, \quad (9)$$

$$Q_e = \frac{V_0 c_0 - V_e c_e}{W}, \quad (10)$$

where V_0, V_t and V_e are the volumes (L) of the initial dye solution, the dye solution at time (t), and the dye solution that reached adsorption equilibrium, respectively; c_0, c_t and c_e are the concentrations (mg·L^{-1}) of the initial dye solution, the dye solution at time t and the dye solution that reached adsorption equilibrium, respectively; W is the weight (g) of the adsorbent. All adsorption experiments were repeated three times to ensure the accuracy of the data, and the results were expressed in terms of average values.

Foam-12 (20 mg) was mixed with 100 mL of 100 mg·L^{-1} AR 134 solution at pH 3.5. The mixture was agitated for 24 h at 25 °C. Deionized water and ethanol were successively used to wash the AR 134-loaded Foam-12. All the filtration and washing lotion were collected and the dye concentration in the mixture was measured as before. The dye amount adsorbed on the foam (Q_e) was calculated by Eq. (10). Next, the dye on the nanocomposite foam was desorbed by soaking it in 100 mL of NaOH solution at pH 8 and agitating at 200 r·min^{-1} with a shaker for 30 min, followed by washing with 0.1 mol·L^{-1} HCl, water, and ethanol and then dry it under vacuum condition. The foam was scheduled for the second adsorption experiment. In this way, the adsorption–desorption experiments were repeated for six times.

3 Results and discussion

3.1 Characterization of PAETMAC-*g*-DACNCs

Results from TEM, FTIR, XRD characterizations are shown in Fig. 1. The calculated mean sizes of nanocrystals in CNCs, DACNCs, and PAETMAC-*g*-DACNCs, the measured aldehyde content, a and ζ-values are listed in Table S1 (cf. Electronic Supplementary Material, ESM).

As exhibited in Fig. 1(a), rod-like nanoparticles are observed in TEM images of all samples. DACNCs present largely smaller particles than CNCs, which is due to gradual destruction of crystals during the periodate-oxidation of CNCs [22,26]. As shown in Table S1, the mean sizes of CNCs and DACNCs are 343.4 and 101.6 nm, respectively. After the PAETMAC side chains incorporation into the DACNC surface, the product of

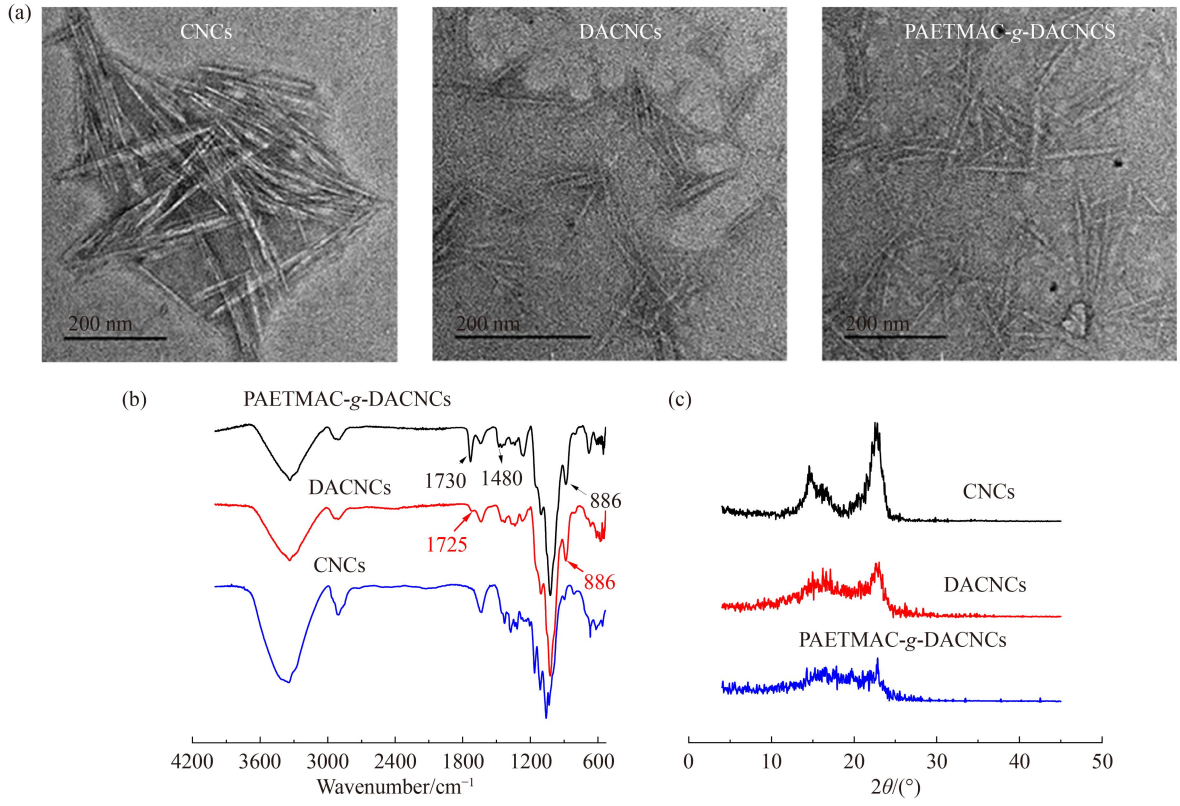

Fig. 1 (a) TEM images, (b) FTIR spectra, and (c) XRD patterns of CNCs, DACNCs and PAETMAC-*g*-DACNCs.

PAETAC-*g*-DACNCs becomes larger (137.2 nm). It is worth noting that the particles in the TEM image of PAETMAC-*g*-DACNCs are much larger than that of DACNCs, which is not in agreement with the results from the particle size test. This is possibly due to the presence of both positive and negative charges on the surface of PAETMAC-*g*-DACNCs, and thus the electrostatic attraction between nanoparticles promotes their aggregation.

A comparison of FTIR spectrum of DACNCs with that of CNCs in Fig. 1(b), reveals that there is a weaker band of hydroxyls at about 3330 cm^{-1}, new bands of aldehyde carbonyl groups at 1725 cm^{-1} and hemiacetals at 886 cm^{-1}. These provide sufficient evidence for the conversion of hydroxyls into aldehydes and/or hemiacetals on nanocrystal surface during the oxidation of CNCs by $NaIO_4$. After comparing the FTIR spectrum of PAETMAC-*g*-DACNCs with that of DACNCs in Fig. 1(b), there are two new bands at 1730 cm^{-1} (overlapped with the band of aldehyde carbonyl groups at 1725 cm^{-1}) of saturated ester linkage (CH_2–CH–C(=O)–O), 1480 cm^{-1} of methyl groups (CH_3) of ammonium [19,23]. It is suggested that the cationic moieties of PAETMAC side chains have been introduced onto nanocrystal surface. Otherwise, the absorption band of hemiacetals at 886 cm^{-1} still exists in the FTIR spectrum of PAETMAC-*g*-DACNCs. It remains approximate intensity to that in the FTIR spectrum of DACNCs. All these imply that PAETMAC-*g*-DACNCs contain both cationic moieties and reactive aldehydes. As also seen in Fig. 1(b), DACNCs possess weaker bands of cellulose at 900–1500 cm^{-1} than CNCs. PAETMAC-*g*-DACNCs have almost unchanged bands of cellulose as DACNCs. This means that a serious decomposition of cellulose takes place during the periodate oxidation of CNCs. Whereas, the degradation of cellulose was very slight in the subsequent graft modification of DACNCs.

The crystallographic planes of cellulose I ((10), (110) and (200)) are found at 2θ 14.5°, 16.5° and 22.6°, respectively, in XRD pattern of CNCs (Fig. 1(c)). Comparatively, XRD pattern of DACNCs shows no major change in diffraction angle but an obvious decrease in diffraction intensity. Herein, it is proved again that the crystalline region is disrupted to some degree by cellulose degradation during the periodate oxidation of CNCs [22,26]. The *CrI* value of DACNCs, 52.4%, is obviously lower than that of CNCs, 87.8%. The *CrI* value of PAETMAC-*g*-DACNCs is 45.5%, which is somewhat lower than that of DACNCs. This is consistent with the results of the previous FTIR analysis.

As shown in Table S1, the free aldehyde content of PAETMAC-*g*-DACNCs, 5.3 mmol·g^{-1}, is slightly less than that of DACNCs, 5.9 mmol·g^{-1}. This explains that the free radical polymerization of AETMAC occurs at the surface hydroxyls on DACNCs and most of the free aldehydes on DACNCs are kept unreacted. Under these circumstances, PAETMAC-*g*-DACNCs can cross-link with chitosan, generating the cross-linking networks in the nanocomposites. The periodate-oxidation of CNCs

would reduce the amount of surface sulfate ester groups. Accordingly, the ζ-value of DACNCs suspension is different from that of CNC suspension. The ζ-values of DACNC and CNCs suspensions are –20.3 and –38.3 mV, respectively. On the contrary, the suspension of PAETMAC-*g*-DACNCs has positive charges of +28.3 mV. Adding to this, the *a* value of PAETMAC-*g*-DACNCs is 9.1%. These infer again that the quaternary ammonium groups have been grafted onto nanocrystal surface, and they are prominent over sulfate ester groups. On account of that, flocs will be avoided in the mixture of PAETMAC-*g*-DACNCs suspension and chitosan acetic acid solution [23].

3.2 Characterization of the nanocomposite foams

After mixing the PAETMAC-*g*-DACNC suspension with the acetic acid solution of chitosan, hydrogels gradually form. The hydrogels are further turned into nanocomposite foams. The cross-link between PAETMAC-*g*-DACNCs and chitosan is expected to improve the acid resistance of nanocomposite foam, but at the same time, it may decrease the dye accessibility. On these grounds, the lower degree of cross-linking between PAETMAC-*g*-DACNCs and chitosan is more beneficial for dye adsorption on the premise of ensuring the acid stability of nanocomposite foam. Hence, it is essential to confirm the occurrence and degree of cross-linking between PAETMAC-*g*-DACNCs and chitosan in these nanocomposite foams. Only in this way can we further know more about the prepared nanocomposite foam, such as the porosity, crystalline structure, and saturated swelling ratio immersed in water. Similarly, these are crucial for the dye adsorption properties of nanocomposite foam.

3.2.1 Characterization of cross-linking between PAETMAC-*g*-DACNCs and chitosan

Photographs of the formed hydrogels from the five mixtures of the PAETMAC-*g*-DACNC suspension and the chitosan acetic acid solution (PAETMAC-*g*-DACNCs/chitosan (w/w): 0/100, 3/100, 6/100, 9/100 and 12/100), the weight percentages of glucosamine in the nanocomposite foams, FTIR spectra, and XRD patterns of the nanocomposite foams are exhibited in Fig. 2.

As seen in Fig. 2(a), the mixture fluidity changes until the hydrogel is formed. That is, the cross-linking between PAETMAC-*g*-DACNCs and chitosan ultimately leads to a stable three-dimensional network as schemed in Scheme 1, which can lock a tremendous amount of water. With the increase of PAETMAC-*g*-DACNCs loading in the mixture, the degree of cross-linking between chitosan and PAETMAC-*g*-DACNCs in the hydrogel or the nanocomposite foam enhances. As a result, a more cross-linked network facilitates the formation of a more stable hydrogel. All hydrogels are frozen dried to form the nanocomposite foams, as also schemed in Scheme 1.

As seen in Fig. 2(b), the characteristic absorption peaks of chitosan at 3200–3450 (O–H stretching overlapped with N–H stretching), 1642 (C=O stretching) and 1548 cm^{-1} (N–H bending) appear in the FTIR spectra of all samples, giving rise to the main component of chitosan moieties in the nanocomposite foams. Besides, a peak at about 1736 cm^{-1} appears in Foam-3 to Foam-12

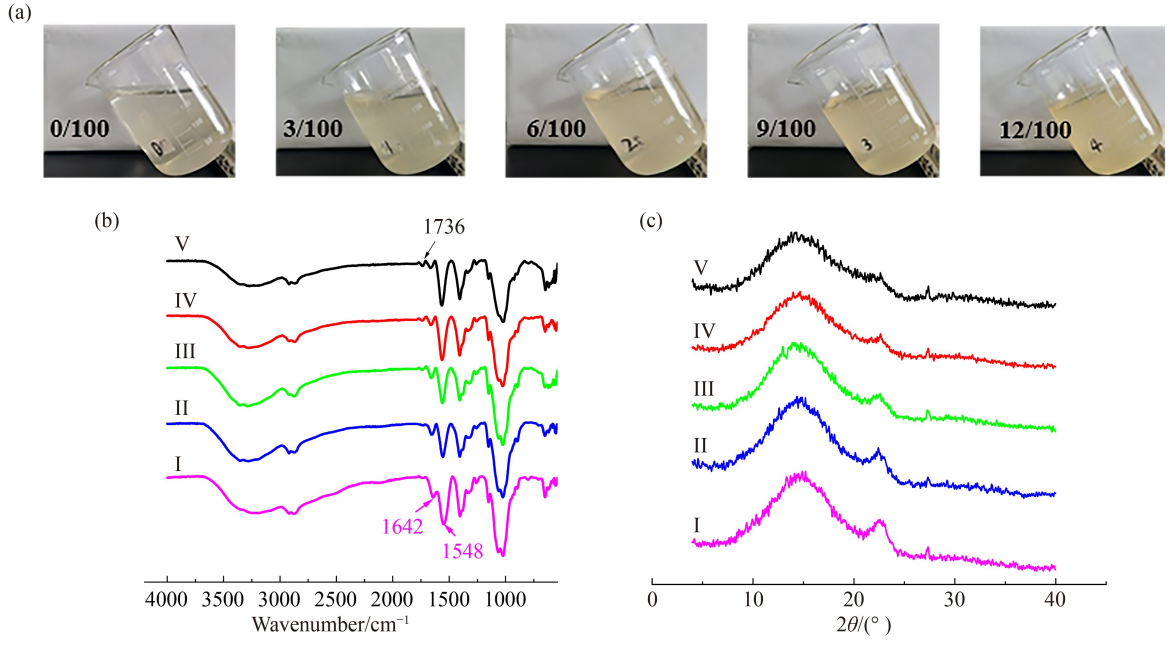

Fig. 2 (a) Photographs of the mixture of PAETMAC-*g*-DACNCs suspension and chitosan acetic acid solution stored at 25 °C for 24 h; (b) FTIR spectra and (c) XRD patterns of chitosan foam and the PAETAMC-*g*-DACNCs/chitosan nanocomposite foams (the curves marked as I, II, III, IV and V are composites with proportion of 0/100, 3/100, 6/100, 9/100 and 12/100, respectively).

but is absent in the pure Foam-0, confirming the successful loading of PAETMAC-*g*-DACNCs in the nanocomposite foams. The intensity of this peak is proportional to the loading amount of PAETMAC-*g*-DACNCs in the nanocomposite foams.

The nanocomposite foam with the higher weight percentage of PAETMAC-*g*-DACNCs shows a rising ratio of peak intensity at 1548 cm^{-1} to that at 1642 cm^{-1} in the corresponding FTIR spectrum, which might be assigned to the formation of C=N bond in imines. It can be derived that the Schiff-base reaction between the aldehydes on PAETMAC-*g*-DACNCs and the glucosamines in chitosan promotes establishing the chemically cross-linked networks in the PAETMAC-*g*-DACNCs/chitosan nanocomposite foam [27].

As seen in Fig. 2(c), the diffraction intensity of crystalline peaks at 2θ = 15.6° and 22.6° is weakened with increasing the loading of PAETAMC-*g*-DACNCs in the corresponding nanocomposite foam. Consequently, the crystallization of chitosan is impeded by its cross-linking reaction with PAETMAC-*g*-DACNCs. The higher weight percentage of PAETMAC-*g*-DACNCs relative to chitosan causes the higher cross-linking degree between PAETMAC-*g*-DACNCs and chitosan, and the crystallization of chitosan becomes more difficult. Namely, the corresponding nanocomposite foam has a more amorphous region, which makes the adsorption sites more accessible.

The weight percentages of glucosamine in the pure chitosan foam and the PAETMAC-*g*-DACNCs/chitosan nanocomposite foams were measured by using pH-titration [12]. The pH-titration diagrams are presented in Fig. 3.

As seen in Fig. 3, the NaOH consumption between the first and second jumping points in the figure decreases in the order of Foam-0, Foam-3, Foam-6, Foam-9 and Foam-12, implying that the glucosamine amount in the nanocomposite foam decreases with increasing loading of PAETMAC-*g*-DACNCs. The W_{NH_2} values calculated by

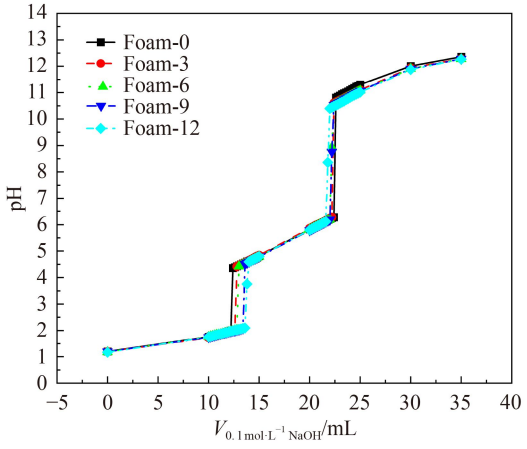

Fig. 3 The pH-titration diagrams of the pure chitosan foam and the PAETMAC-*g*-DACNCs/chitosan nanocomposite foams.

Eq. (4) and the D_c values calculated by Eq. (5) were listed in Table S2 (cf. ESM).

As shown in Table S2, the other four foams bear less glucosamine than the pure chitosan foam, because some chitosan is reacted with the aldehyde groups on PAETMAC-*g*-DACNCs. Adding more PETMAC-*g*-DACNCs relative to chitosan in the mixture, more glucosamine groups in chitosan are consumed, bringing on higher cross-linking degree between PAETMAC-*g*-DACNCs and chitosan in the nanocomposite foam. Yet the cross-linking degrees between PAETMAC-*g*-DACNCs and chitosan in all the nanocomposite foams are generally low (< 25%), illustrating that the glucosamine amount in each nanocomposite foam is kept at a relatively high level. In another word, most of the glucosamine groups in chitosan are remained in the nanocomposite foam, although part of them participates in the cross-linking reaction.

3.2.2 Acid resistance of nanocomposite foams

As discussed above, the PAETMAC-*g*-DACNC filled and cross-linked chitosan nanocomposite foams are promising adsorbents for the removal of anionic dyes from aqueous solutions and will have high adsorption efficiency, as long as they can meet the requirements of acid stability in actual water. The acid stability of them was analyzed based on the water swelling tests. The saturated swelling ratio of each sample immersed in water at different pH is listed in Table 1. The photographs of five foams immersed in water at pH 3.5 for 24 h were taken and shown in Fig. S1 (cf. ESM).

The pure chitosan foam is dissolved at both pH 3.5 and pH 5.0, so it gives no data on the saturated swelling ratio under these conditions. As seen in Table 1, the saturated water swelling ratio of the foams is depended on the cross-linking degree between PAETMAC-*g*-DACNCs and chitosan plus the water pH value. At given pH, the higher the cross-linking degree, the lower the water swelling ratio at saturation, because the cross-linked chemical bonds block the hydrophilic sites of chitosan in the nanocomposite foam, and fewer glucosamine groups are left to interact with water molecules. Such behavior was also found for the genipin-cross-linked carboxymethylchitosan porous membranes [15]. No matter what

Table 1 The swelling ratios of the pure chitosan foam and the PAETMAC-*g*-DACNCs/chitosan nanocomposite foams immersed in water at different pH for 24 h

The proportion of PAETMAC-*g*-DACNCs to chitosan in the nanocomposite foams	Swelling ratio/%		
	pH = 3.5	pH = 5	pH = 6.5
0/100 (Foam-0)	–	–	1107
3/100 (Foam-3)	4088	2365	1029
6/100 (Foam-6)	3835	2218	1019
9/100 (Foam-9)	2945	2112	980
12/100 (Foam-12)	2764	1999	913

kind of nanocomposite foam is used, the higher swelling ratio at saturation is achieved when it is immersed in water at a lower pH value because more protonated glucosamine groups in chitosan add to the hydrophilic site of the nanocomposite foam. Evidently, the saturated water swelling ratio at pH 3.5 is higher than that of pH 6.5, manifesting that the glucosamine groups in the nanocomposite foam can be more easily accessed by anionic dyes at a higher acidic medium.

As seen in Fig. S1, Foam-0 dissolves when it has been immersed in water at pH 3.5 for 24 h. In contrast, the PAETMAC-*g*-DACNCs filled and cross-linked chitosan nanocomposite foams only swell but do not dissolve under the same conditions. Hereby, the PAETMAC-*g*-DACNCs filled and cross-linked chitosan nanocomposite foams fabricated in this study can be potentially applied in water-related fields, i.e., the adsorption of anionic dyes from acid effluents.

3.2.3 Pore morphology and porosity of nanocomposite foams

SEM images of the fractured cross-sections of the pure chitosan foam and the PAETMAC-*g*-DACNCs filled and cross-linked chitosan nanocomposite foams are exhibited in Fig. 4.

As seen in Fig. 4, macro-pores in a diameter smaller than 500 μm are observed in SEM images of the five samples. In general, the nanocomposite foam with higher PAETMAC-*g*-DACNCs loading has relatively smaller pores. Moreover, these pores are interconnected. The porosities of Foam-0, Foam-3, Foam-6, Foam-9 and Foam-12 are 97.4%, 96.8%, 96.1%, 95.6% and 95.1%, respectively, according to the ethanol adsorption test. Clearly, the nanocomposite foam with higher content of PAETMAC-*g*-DACNCs, in which the cross-linking degree between PAETMAC-*g*-DACNCs and chitosan is

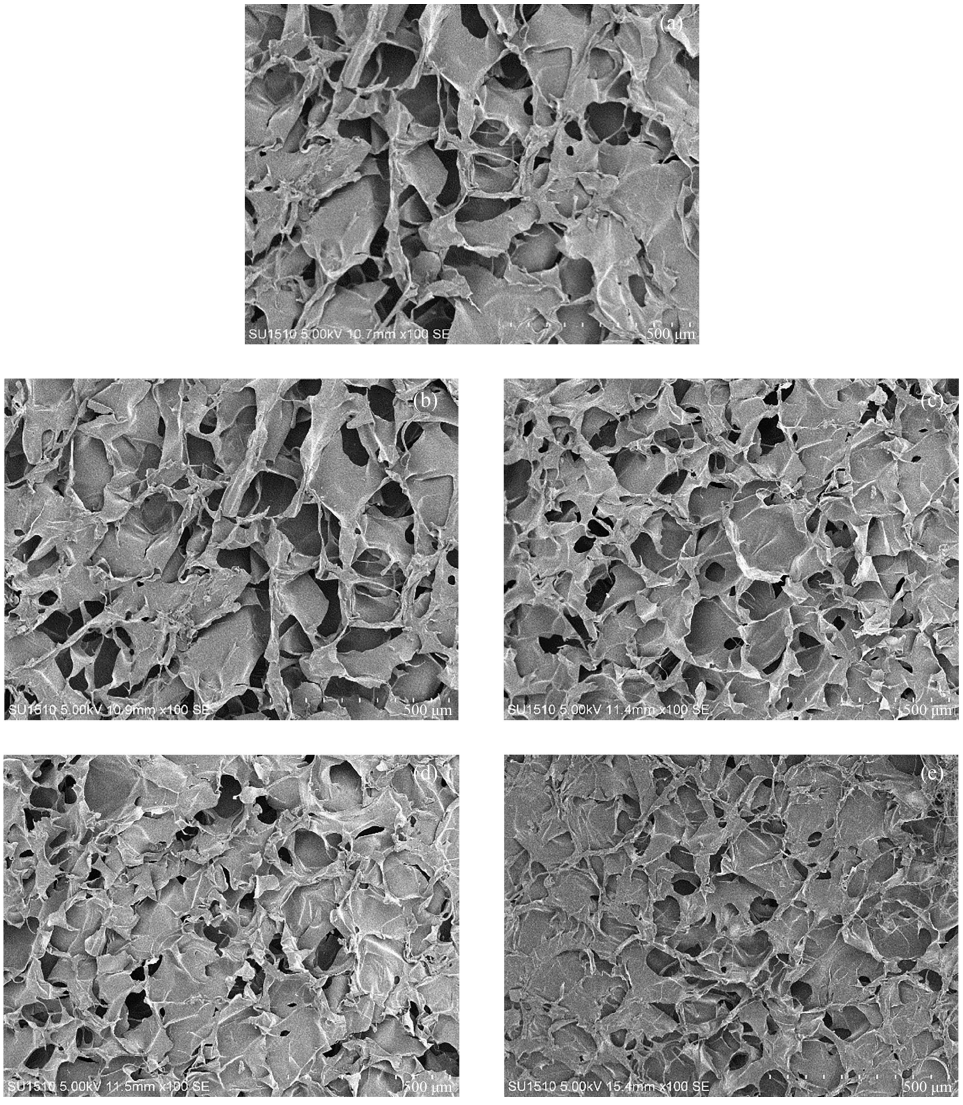

Fig. 4 SEM images of the cross-sections of the composite foams with PAETMAC-*g*-DACNCs/chitosan ratios of (a) 0/100, (b) 3/100, (c) 6/100, (d) 9/100, and (e) 12/100.

higher, has slightly decreased porosity. However, the porosity of each sample is kept higher than 95%. The high porosity makes the active sites of both glucosamine and quaternary ammonium groups in the nanocomposite foam more accessible for the immobilization of dyes and thus are in favor of dye adsorption.

3.3 Adsorption and desorption behaviors of Foam-12 toward AR 134

The adsorption efficiency of an absorbent is affected by many factors, e.g., the amounts of active sites for immobilization of dyes, the crystallinity, and the porosity. Among the fabricated nanocomposite foams, Foam-12 has been manifested to have high glucosamine percentage (64.4%) and porosity (95.1%). Meanwhile, it has the best acid stability and the lowest crystallinity. Correspondently, Foam-12 was chosen as a representative of the PAETMC-*g*-DACNCs filled and cross-linked chitosan nanocomposite foams to investigate the dye (AR 134) adsorption and desorption properties.

3.3.1 Effect of pH on the adsorption of Foam-12 toward AR 134

The dye uptake and the dye removal percentage of Foam-12 at different pH is presented in Fig. 5.

Either the dye uptakes or the dye removal percentages of Foam-12 are high in the pH ranges from 2.5 to 5.5, indicating the high adsorption efficiency of Foam-12 toward AR 134 in acid water. As seen in Fig. 5, both the dye uptakes and the dye removal percentages of Foam-12 reach the maximal value at pH 3.5. When the pH of the initial dye solution is over 3.5, fewer glucosamine groups are protonated, weakening their interaction with the anionic sulfonic groups of dyes. Therefore, the dye uptake is reduced when the pH of the initial dye solution is increased from 3.5 to 5.0. When the solution pH is very low (pH < 3.5), the dye uptake decreases with the decrease of pH from 3.5 to 2.5. Under this condition, the anionic sulfonic groups of AR 134 (Dye-SO_3^-) are converted into Dye-SO_3H. Less negative charges of dyes weaken dyes' binding with the given adsorbent. In view of these points, the dominant role for dyes' adsorption onto the given adsorbent is electrostatic attraction, which will be further manifested by the isotherms and kinetics of adsorption.

3.3.2 Adsorption kinetics of Foam-12 toward AR 134

The AR 134 adsorption kinetics onto Foam-12, the linear plots of t/Q_t vs t and $\ln(Q_e-Q_t)$ vs t are shown in Fig. 6.

To linearly simulate the data in Fig. 6(a), the pseudo-first-order and pseudo-second-order kinetic models as Eqs. (11) and (12) were adopted:

$$\ln(Q_e - Q_t) = \ln Q_e - k_1 t, \tag{11}$$

$$\frac{t}{Q_t} = \frac{1}{k_2 Q_e^2} + \frac{1}{Q_e} t, \tag{12}$$

where Q_e and Q_t (mg·g^{-1}) are the adsorption capacities at equilibrium and the adsorption capacity at time t (min); k_1 (min^{-1}) is the rate constant for the pseudo-first-order model and k_2 (g·mg^{-1}·min^{-1}) is the rate constant for pseudo-second-order model [22,26].

The kinetic parameters calculated from the intercepts and slopes of the linear plots of t/Q_t vs t (Fig. 6(b)) and $\ln(Q_e-Q_t)$ vs t (Fig. 6(c)) are summarized in Table S3 (cf. ESM). The correlation coefficient (R^2) values shown in Table S3 explain that the adsorption of AR 134 onto Foam-12 is better described by the pseudo-second-order kinetic model. And the rate-controlling step in dyes' adsorption is chemisorption based on the sharing or exchange of electrons between the adsorbent and adsorbates. This result is consistent with the kinetic

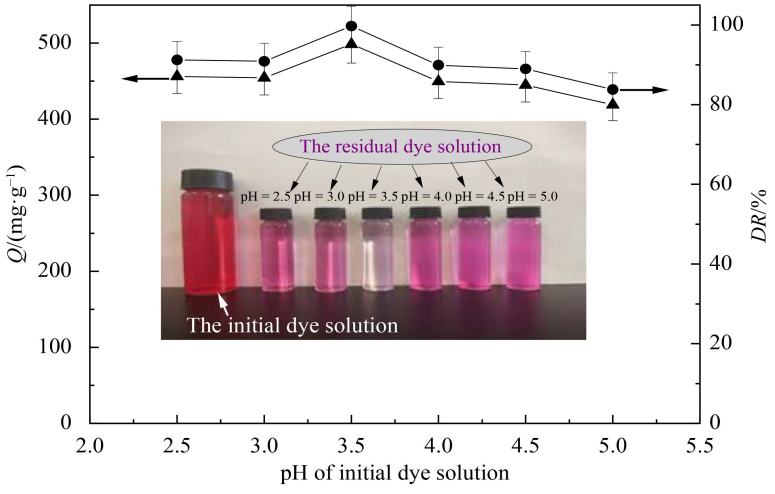

Fig. 5 The dye uptake and the dye removal percentage of 12/100 PAETMAC-*g*-DACNCs/chitosan (Foam-12) at different pH of the initial dye solution (adsorbent dose = 200 mg·L^{-1}; dye concentration = 100 mg·L^{-1}; solution temperature = 25 °C).

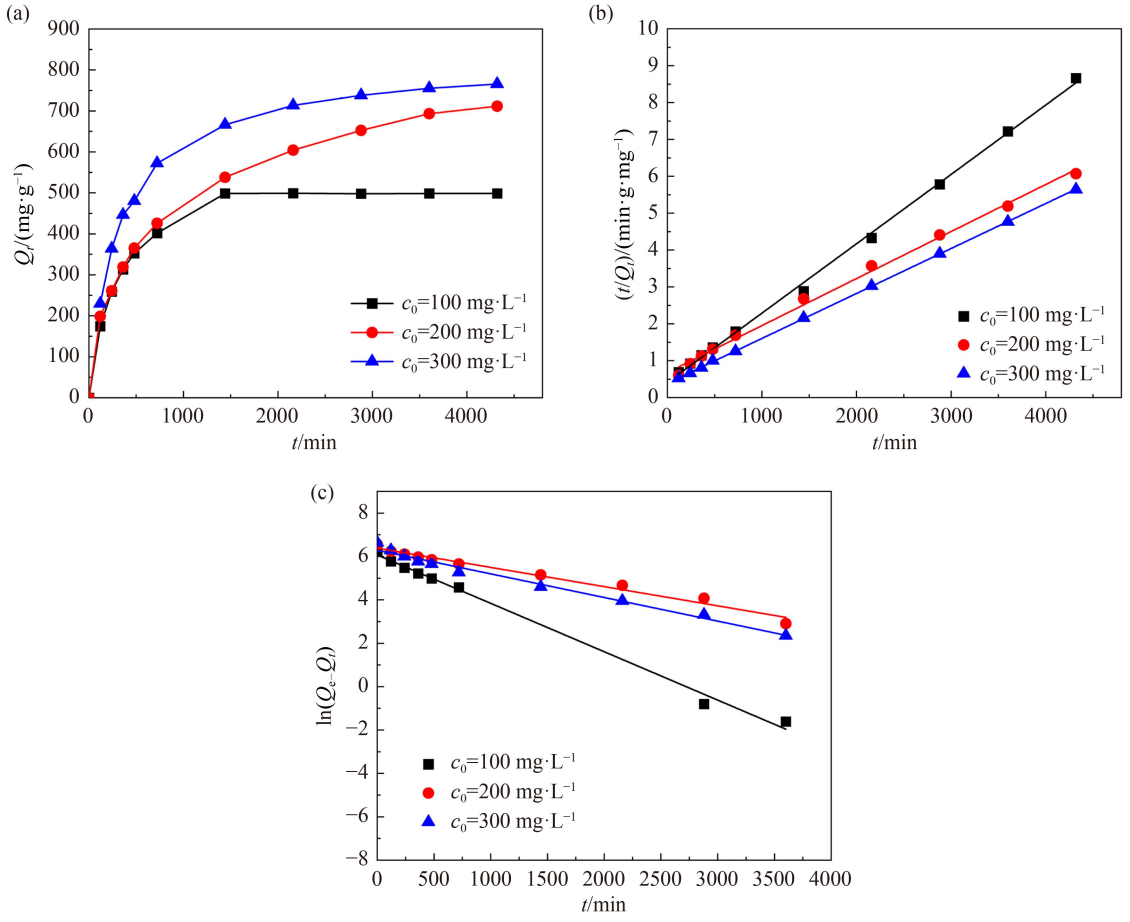

Fig. 6 The relation curves between adsorption capacity and time at different concentrations: (a) the adsorption capacity of 12/100 PAETMAC-*g*-DACNCs/chitosan (Foam-12) toward AR 134 at varied time, and (b) the linear plots of t/Q_t vs t and (c) the linear plots of $\ln(Q_e - Q_t)$ vs t.

model fitting results of various pollutant-adsorbent systems [28–32].

3.3.3 Adsorption isotherm of Foam-12 toward AR 134

The equilibrium isotherm of Foam-12 toward AR 134, the linear plots of $1/Q_e$ vs $1/c_e$ and $\log Q_e$ vs $\log c_e$ are presented in Fig. 7.

To linearly simulate the data in Fig. 7(a), both Langmuir and Freundlich adsorption isotherms as Eq. (13) and Eq. (14), respectively [33], were utilized:

$$\frac{1}{Q_e} = \frac{1}{Q_m} + \frac{1}{C_e Q_m b}, \tag{13}$$

$$\log Q_e = \log k_f + \frac{1}{n}\log c_e, \tag{14}$$

where Q_m is the maximum adsorption capacity (mg·g^{-1}) according to monolayer adsorption and b is the Langmuir adsorption constant (L·mg^{-1}); k_f is the Freundlich adsorption constant ((mg·g^{-1})·(L·mg^{-1})$^{1/n}$) and n is the Freundlich adsorption exponent.

The isotherm parameters calculated from the intercepts and slopes of the linear plots of $1/Q_e$ vs $1/c_e$ in Fig. 7(b) and $\log Q_e$ vs $\log c_e$ in Fig. 7(c), are summarized in Table S4 (cf. ESM). The correlation coefficient (R^2) value from the linear simulation of the Langmuir model is 0.9999, which is higher than that of the Freundlich model, 0.8621. Accordingly, the adsorption of AR 134 onto Foam-12 is accordant with the Langmuir model. It is a monolayer coverage and is controlled by the electrostatic attraction between the cationic groups in nanocomposite foam ($-^{+}NH_3$) and the anionic groups in AR 134 ($-SO_3^-$). Based on the Langmuir model, the maximum AR 134 adsorption capacity of Foam-12 is 1238.1 mg·g^{-1}, which is in accordance with the literature [34,35].

3.3.4 The pH responsive dye adsorption and desorption of Foam-12

As demonstrated before, the mechanism of AR 134 adsorption onto Foam-12 is electrostatic attraction. This is the base for the pH responsiveness of dye adsorption and desorption. The schematic pH responsiveness of AR 134 adsorption and desorption using Foam-12 and the uptake of AR 134 on Foam-12 over a few successive acid adsorption−alkaline desorption cycles are displayed in Fig. 8.

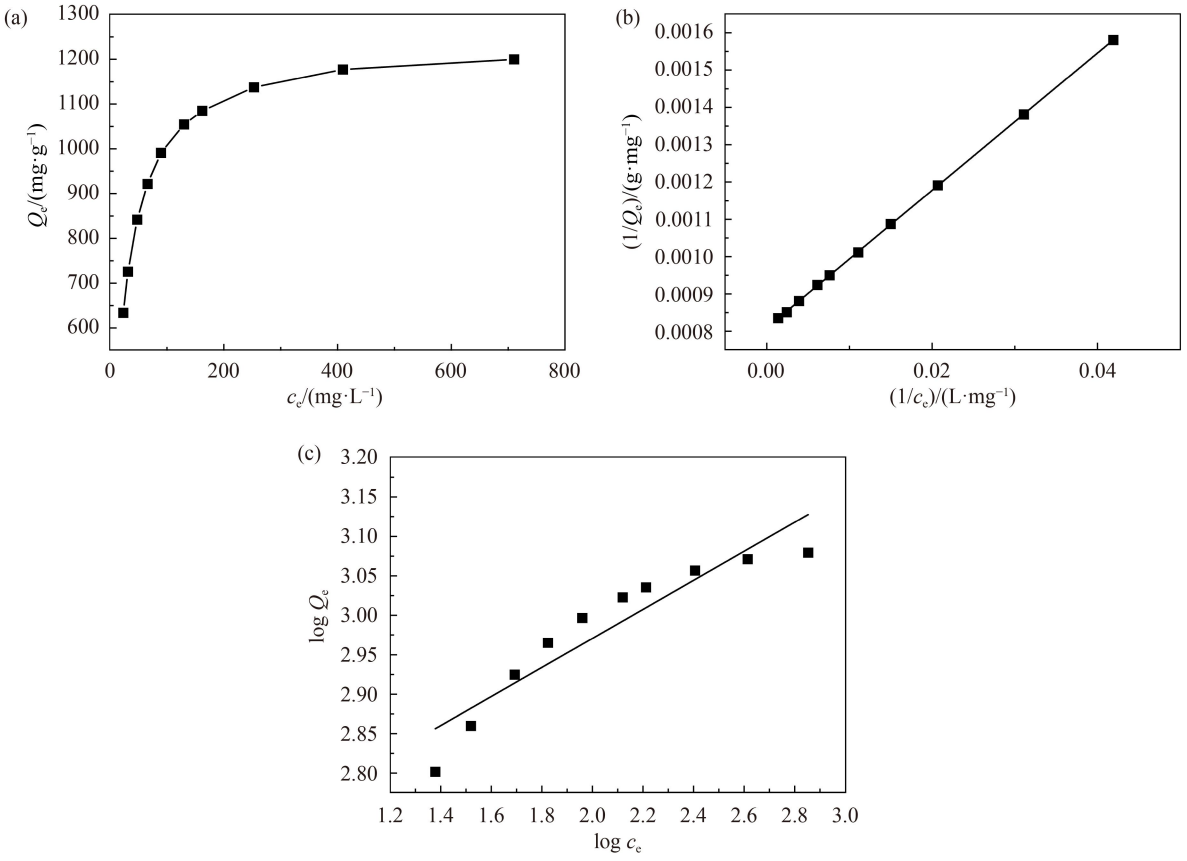

Fig. 7 (a) Adsorption isotherm for AR 134 onto Foam-12, (b) linear plot of $1/Q_e$ vs $1/c_e$, and (c) linear plot of $\log Q_e$ vs $\log c_e$.

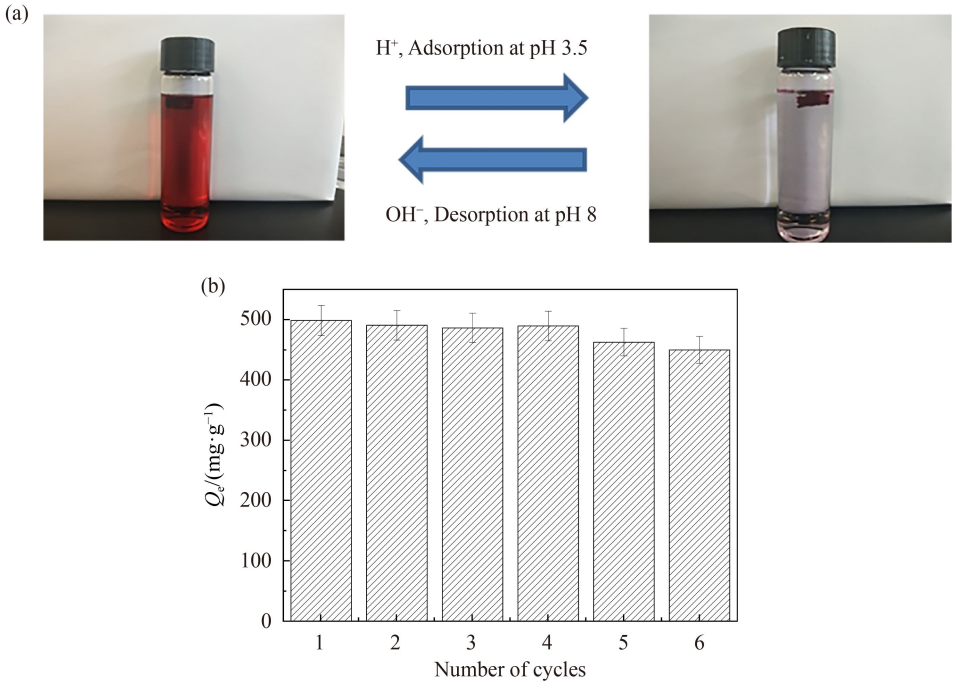

Fig. 8 (a) Schematic pH responsiveness of AR 134 adsorption and desorption using Foam-12, and (b) the uptake of AR 134 on Foam-12 over a few successive acid adsorption−alkaline desorption cycles.

As shown in Fig. 8(b), the dye uptake after four cycles remains almost constant, higher than 98.0% of the initial dye uptake. It decreases in the subsequent fifth cycle from 489.5 to 462.5 mg·g^{-1}, which is about 92.8% of the initial

dye uptake. It is still maintained about 90.2% of the initial adsorption capacity after six cycles, which testifies excellent recyclability of the Foam-12 for the adsorption of AR 134 from aqueous solution.

4 Conclusions

PAETMAC-*g*-DACNCs bearing both aldehyde and cationic groups were first synthesized and verified based on the results from the *a* and *ζ*-values, particle size, FTIR spectra, and XRD analyses. Subsequently, bio-based foam materials were prepared by mixing PAETMAC-*g*-DACNCs with chitosan, and PAETMAC-*g*-DACNCs function as both fillers and cross-linkers. SEM images of the resultant foams indicate that inter-connected macro-pores with diameters of lower than 500 μm are abundant. FTIR and XRD characterizations, together with the glucosamine weight percentage measurements, support the conclusion that cross-linking does occur between PAETMAC-*g*-DACNCs and chitosan in the nanocomposite foams. An increase in the PAETMAC-*g*-DACNCs/chitosan weight ratio results in more cross-linked networks, producing nanocomposite foam with stronger acid resistance, and a more amorphous region. Foam-12 has the most amorphous region, strongest acid stability, as well as high porosity and high content of active sites, and it was studied as an adsorbent for AR 134 dye at pH 3.5. The highest adsorption capacity of 1238.1 $mg \cdot g^{-1}$ was achieved under the conditions: 20 mg of adsorbent, 100 $g \cdot L^{-1}$ dye concentration, 25 °C, pH 3.5, and 24 h. Furthermore, the dye-loaded nanocomposite foam can be easily regenerated at pH 8. After 6 cycles of acidic adsorption (pH 3.5) and alkaline desorption (pH 8), the dye adsorption capacity remains at 90.2% of that of the pristine Foam-12.

Acknowledgements This work was supported by the Natural Science Advance Research Foundation of Shaanxi University of Science and Technology (Grant No. 2020XSGG-07), the Key Research and Development Program of Shaanxi Province (Grant No. 2022GY-278) and the Natural Science Basic Research Program of Shannxi (Program No. 2023-JC-YB-104).

Electronic Supplementary Material Supplementary material is available in the online version of this article at https://dx.doi.org/10.1007/s11705-022-2256-x and is accessible for authorized users.

References

1. Holkar C R, Jadhav A J, Pinjari D V, Mahamuni N M, Pandit A B. A critical review on textile wastewater treatments: possible approaches. Journal of Environmental Management, 2016, 182: 351–366
2. Hao X, Chen G, Yuan Z. Water in China. Water Research, 2019, 169: 115256
3. Rodrigues C S D, Madeira L M, Boaventura R A. Decontamination of an industrial cotton dyeing wastewater by chemical and biological processes. Industrial & Engineering Chemistry Research, 2014, 53(6): 2412–2421
4. Varjani S, Rakholiya P, Ng H Y, You S, Teixeira J A. Microbial degradation of dyes: an overview. Bioresource Technology, 2020, 314: 123728
5. Wang K X, Wei T T, Li Y N, He L, Lv Y, Chen L, Ahmad A, Xu Y S, Shi Y L. Flocculation-to-adsorption transition of novel salt-responsive polyelectrolyte for recycling of highly polluted saline textile effluents. Chemical Engineering Journal, 2021, 413: 127410
6. Yagub M T, Sen T K, Afroze S, Ang H M. Dye and its removal from aqueous solution by adsorption: a review. Advances in Colloid and Interface Science, 2014, 209: 172–184
7. Ramazani A, Oveisi M, Sheikhi M, Gouranlou F. Natural polymers as environmental friendly adsorbents for organic pollutants such as dyes removal from colored wastewater. Current Organic Chemistry, 2018, 22(13): 1297–1306
8. Bozoğlan B K, Duman O, Tunç S. Preparation and characterization of thermosensitive chitosan/carboxymethylcellulose/scleroglucan nanocomposite hydrogels. International Journal of Biological Macromolecules, 2020, 162: 781–797
9. Bozoğlan B K, Duman O, Tunç S. Smart antifungal thermosensitive chitosan/carboxymethyl cellulose/scleroglucan/montmorillonite nanocomposite hydrogels for onychomycosis treatment. Colloids and Surfaces A: Physicochemical and Engineering Aspects, 2021, 610: 125600
10. Huo M X, Jin Y L, Sun Z F, Ren F, Pei L, Ren P G. Facile synthesis of chitosan-based acid-resistant composite films for efficient selective adsorption properties towards anionic dyes. Carbohydrate Polymers, 2021, 254: 117473
11. Zhao X L, Wang X J, Lou T. Preparation of fibrous chitosan/sodium alginate composite foams for the adsorption of cationic and anionic dyes. Journal of Hazardous Materials, 2021, 403: 124054
12. Salehi E, Soroush F, Momeni M, Barati A, Khakpour A. Chitosan/polyethylene glycol impregnated activated carbons: synthesis, characterization and adsorption performance. Frontiers of Chemical Science and Engineering, 2017, 11: 575–585
13. Ke P, Zeng D L, Xu K, Cui J W, Li X, Wang G H. Preparation of quaternary ammonium salt-modified chitosan microspheres and their application in dyeing wastewater treatment. ACS Omega, 2020, 5(38): 24700–24707
14. Salehi E, Daraei P, Shamsabadi A A. A review on chitosan-based adsorptive membranes. Carbohydrate Polymers, 2016, 152: 419–432
15. Fiamingo A, Campana-Filho S P. Structure, morphology and properties of genipin-crosslinked carboxymethylchitosan porous membranes. Carbohydrate Polymers, 2016, 143: 155–163
16. Yang H, Sheikhi A, Van De Ven T G M. Reusable green aerogels from cross-linked hairy nanocrystalline cellulose and modified chitosan for dye removal. Langmuir, 2016, 32(45): 11771–11779
17. Khapre M A, Pandey S, Jugade R M. Glutaraldehyde-cross-linked chitosan-alginate composite for organic dyes removal from aqueous solutions. International Journal of Biological

Macromolecules, 2021, 190: 862–875

18. Selkala T, Suopajarvi T, Sirvio J A, Luukkonen T, Kinnunen P, de Carvalho A L C B, Liimatainen H. Surface modification of cured inorganic foams with cationic cellulose nanocrystals and their use as reactive filter media for anionic dye removal. ACS Applied Materials & Interfaces, 2020, 12(24): 27745–27757
19. Tian X Z, Hua F, Lou C Q, Jiang X. Cationic cellulose nanocrystals (CCNCs) and chitosan nanocomposite films filled with CCNCs for removal of reactive dyes from aqueous solutions. Cellulose, 2018, 25(7): 3927–3939
20. Xu J F, Li X Y, Xu Y Q, Wang A Q, Xu Z L, Wu X, Li D F, Mu C D, Ge L M. Dihydromyricetin-loaded pickering emulsions stabilized by dialdehyde cellulose nanocrystals for preparation of antioxidant gelatin–based edible films. Food and Bioprocess Technology, 2021, 14(9): 1648–1661
21. Jiang X, Lou C Q, Hua F, Deng H B, Tian X Z. Cellulose nanocrystals-based flocculants for high-speed and high-efficiency decolorization of colored effluents. Journal of Cleaner Production, 2020, 251: 119749
22. Tian X Z, Jiang X. Preparing water-soluble 2,3-dialdehyde cellulose as a bio-origin cross-linker of chitosan. Cellulose, 2018, 25(2): 987–998
23. Tian X Z, Yan D D, Lu Q X, Jiang X. Cationic surface modification of nanocrystalline cellulose as reinforcements for preparation of the chitosan-based nanocomposite films. Cellulose, 2017, 24(1): 163–174
24. Pietrucha K, Safandowska M. Dialdehyde cellulose-crosslinked collagen and its physicochemical properties. Process Biochemistry, 2015, 50(12): 2105–2111
25. Tian X Z, Yang R, Chen T, Cao Y, Deng H B, Zhang M Y, Jiang X. Removal of both anionic and cationic dyes from wastewater using pH-responsive adsorbents of L-lysine molecular-grafted cellulose porous foams. Journal of Hazardous Materials, 2022, 426: 128121
26. Chen D, van de Ven T G M. Morphological changes of sterically stabilized nanocrystalline cellulose after periodate oxidation. Cellulose, 2016, 23(2): 1051–1059
27. Teotia A, Ikram S, Gupta B. Structural characterization of chitosan and oxidized carboxymethyl cellulose based freeze-dried films. Polymer Bulletin, 2012, 69(2): 175–188
28. Ayranci E, Duman O. *In-situ* UV-visible spectroscopic study on the adsorption of some dyes onto activated carbon cloth. Separation Science and Technology, 2009, 44(15): 3735–3752
29. Ayranci E, Duman O. Structural effects on the interactions of benzene and naphthalene sulfonates with activated carbon cloth during adsorption from aqueous solutions. Chemical Engineering Journal, 2010, 156(1): 70–76
30. Li Y X, Yang Z X, Wang Y L, Bai Z L, Zheng T, Dai X, Liu S T, Gui D X, Liu W, Chen M. A mesoporous cationic thorium-organic framework that rapidly traps anionic persistent organic pollutants. Nature Communications, 2017, 8: 1354
31. He L W, Chen L, Dong X L, Zhang S T, Zhang M X, Dai X, Liu X J, Lin P, Li K F, Chen C L. A nitrogen-rich covalent organic framework for simultaneous dynamic capture of iodine and methyl iodide. Chem, 2021, 7(3): 699–714
32. Liang C Y, Cheng L W, Zhang S T, Yang S R, Liu W, Xie J, Chai Z F, Li M D, Wang Y X, Wang S. Boosting the optoelectronic performance by regulating exciton behaviors in a porous semiconductive metal-organic framework. Journal of the American Chemical Society, 2022, 144(5): 2189–2196
33. Jiang X, Sun Y M, Liu L, Wang S G, Tian X Z. Adsorption of C. I. reactive blue 19 from aqueous solutions by porous particles of the grafted chitosan. Chemical Engineering Journal, 2014, 235: 151–157
34. Duman O, Tunç S, Bozoğlan B K, Polat T G. Removal of triphenylmethane and reactive azo dyes from aqueous solution by magnetic carbon nanotube-κ-carrageenan-Fe_3O_4 nanocomposite. Journal of Alloys and Compounds, 2016, 687: 370–383
35. Duman O, Tunç S, Polat T G. Adsorptive removal of triarylmethane dye (basic red 9) from aqueous solution by sepiolite as effective and low-cost adsorbent. Microporous and Mesoporous Materials, 2015, 210: 176–184